The quantum efficiency of HgCdTe photodiodes in relation to the direction of illumination and to their geometry

D. Rosenfeld[a] and G. Bahir
Kidron Microelectronics Research Center, Department of Electrical Engineering, Technion—I.I.T., Haifa, Israel 32000

(Received 6 January 1992; accepted for publication 22 June 1992)

In this paper a theoretical study of the effect of the direction of the incident light on the quantum efficiency of homogeneous HgCdTe photodiodes suitable for sensing infrared radiation in the 8–12 μm atmospheric window is presented. The probability of an excess minority carrier to reach the junction is derived as a function of its distance from the edge of the depletion region. Accordingly, the quantum efficiency of photodiodes is presented for two geometries. In the first, the light is introduced directly to the area in which it is absorbed (opaque region), while in the second, the light passes through a transparent region before it reaches the opaque region. Finally, the performance of the two types of diodes is analyzed with the objective of finding the optimal width of the absorption area. The quantum efficiency depends strongly on the way in which the light is introduced. The structure in which the radiation is absorbed following its crossing the transparent region is associated with both higher quantum efficiency and homogeneity. In addition, for absorption region widths higher than a certain minimum the quantum efficiency in this case is insensitive to the width of the absorption region.

I. INTRODUCTION

The present technology of choice for present and future infrared imaging systems is photovoltaic linear arrays and two-dimensional matrices, which can be coupled with a Si signal processor in the focal plane. The extensive interest in thin films of HgCdTe (either grown on a semi-insulating transparent substrate or thinned from bulk material) is associated with the possibility of illuminating the diodes from one side, and connecting the signal processor on the other side.

For the sake of simplicity we shall consider here only diodes in which the photocurrent is dominated by the contribution of photons absorbed only in one side of the diode. This is frequently the case that occurs when the diffusion length in one side of the junction is very short, or when one of the sides is either based on a wide-band-gap material or is too thin to absorb a significant number of photons. Hence, the photodiodes considered here are based on two different quasineutral regions—a transparent region and an opaque region in which the light is absorbed.

Theoretical and technological considerations usually dictate whether to realize frontside-illuminated diodes with a backside signal processor, or backside-illuminated diodes with a frontside signal processor. However, the analysis shows that the crucial parameter determining the quantum efficiency is the distance of the absorption site from the edge of the depletion region, rather than the side of illumination.

Our investigation will focus on two structures shown in Fig. 1. In the first one, presented in Fig. 1(a), the light reaches the transparent side first (TSF), passes through it and through the depletion region and then is absorbed in the opaque side. In the second structure [Fig. 1(b)], the light reaches the opaque side first (OSF), is partly absorbed there, and only then passes through the depletion region and reaches the transparent side.

Most of the present HgCdTe photodiodes fabricated for the purpose of thermal imaging are included within the above two categories as, for example, the following.

Ion-implanted n^+p photodiodes fabricated on a thin HgCdTe film: due to the small thickness of the implanted n^+ region and to the low-minority-carrier lifetime there, the contribution of the n^+ side to the photocurrent is negligible. As demonstrated by Fig. 1, backside illumination is associated with the OSF configuration, while the frontside illumination is associated with the TSF configuration.

Pn or *Np* diodes realized on heterostructures: usually a structure of a thin narrow-band-gap material layer between a thin wide-band-gap material layer and a semi-insulating transparent substrate. In the case of a one-dimensional array the light can be introduced from either sides of the diodes, while in the case of two-dimensional arrays the light is usually introduced through the semi-insulating substrate (OSF configuration). Regardless of the direction of the illumination, photons with longer wavelengths are absorbed in the narrow-band-gap material only.

Hg-diffused diodes: realized by diffusing Hg into a heavily doped p-type material, forming a thin n-type area. Due to the short minority-carrier lifetime in the p side, the photocurrent is dominated by the contribution of the light absorbed in the n side. The Hg-diffused diodes are usually illuminated through the n side (therefore, OSF). In the case of a thin epitaxially grown p layer the diodes can be illuminated from the opposite side as well (TSF).

In this paper we present a theoretical study of the quantum efficiency of photodiodes fabricated on homogeneous thin films, to determine which of the two geometries renders higher quantum efficiency. Other figures of merit,

[a]Current address: NASA Lewis Research Center, 21000 Brookpark Rd., M/S 54-5, Cleveland, OH 44135.

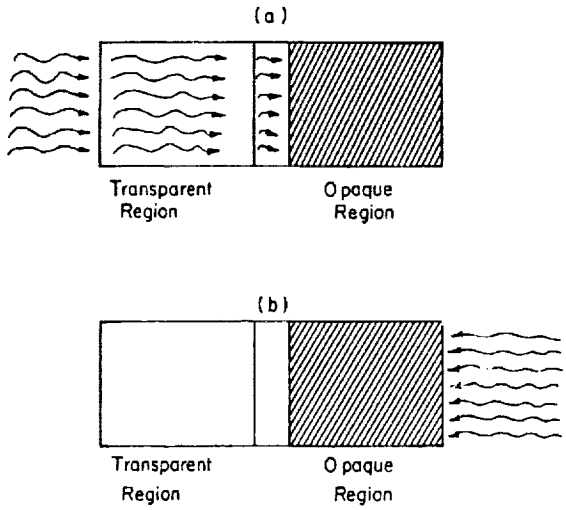

FIG. 1. The two geometrical instances of illumination: (a) the transparent side first (TSF) case, and (b) the opaque side first (OSF) case.

such as noise equivalent temperature difference (NETD) and D_λ^* are proportional to the quantum efficiency. For instance, in the case of background limited-in-performance (BLIP) operation, D_λ^* is given by

$$D_\lambda^* = \frac{R(\lambda)}{[2q(I_d+I_\lambda)]^{1/2}} \cong \frac{\eta(\lambda)\lambda}{hC(2A_d N_0 \eta_{av})^{1/2}}, \quad (1)$$

where R is the responsivity of the photodiode, I_d and I_λ present the dark current and photocurrent, A_d is the detector's optical area, and N_0 is the photon flux. q,h, and c are constant with their regular meaning. $\eta(\lambda)$ and η_{av} represent the quantum efficiency at wavelength λ and the average quantum efficiency in the relevant spectral region.

The effect of the structure of the device on the quantum efficiency, and the correlation between the quantum efficiency and other figures of merit of the photodiodes, have led to the publication of many works in the literature. van der Wiele[1] solved the one-dimensional diffusion equation in silicon, and presented the quantum efficiency associated with both frontside and backside illuminations. More recently, Rogalsky and Rutkowsky[2] used the above-mentioned equations, and analyzed the quantum efficiency of a PbSnTe one-dimensional diode. Other interesting works are those by Shappir and Kolodny,[3] Levy, Schacham, and Kidron,[4,5] and Briggs[6] who, based on numerical and analytical approaches, presented computer solutions for the two-dimensional and three-dimensional cases.

Most of the published works do not deal with HgCdTe in particular, and therefore rightly ignore the asymmetrical structure which characterize the HgCdTe diodes. Their published analytical equations, for both frontside or backside cases, are rather complicated and therefore the geometrical dependence is concealed. In addition, the wavelength dependence of the absorption coefficient is usually ignored. Levy and co-workers[4,5] did not ignore both the wavelength dependence of the absorption coefficient and the geometrical effects; however, their approach, based on two-dimensional Fourier series, totally concealed the geometrical dependence of the quantum efficiency.

One of the objectives of the theoretical study presented here is to emphasize the geometrical dependence of the quantum efficiency in homogeneous photodiodes and to determine whether the OSF or TSF illumination is preferable. We therefore present in Sec. II a one-dimensional analytical equation which describes the probability of the minority carriers generated at a known distance from the edge of the depletion region, to reach the junction and to participate in the photocurrent. We show that this probability depends strongly on the distance of the absorption site from the edge of the depletion region, and emphasize the importance of absorption close to the junction. In Sec. III we use the above-calculated probability, and Plank's radiation law, and compute the quantum efficiency of OSF and TSF HgCdTe photodiodes in the 8–12 μm region. In Sec. IV we demonstrate the superiority of the TSF geometry by presenting an example based on two HgCdTe photodiodes.

Our study does not take into account effects caused by variation in composition or doping which sometimes occur close to the junction. Thin layers grown by liquid-phase epitaxy and more recently by molecular-beam epitaxy (MBE) or metalorganic chemical-vapor deposition (MOCVD) have composition variation throughout the layer. The resulting electric field accelerates minority carriers toward the junction, regardless of the direction of the illumination, and therefore yields higher quantum efficiencies in both OSF and TSF photodiodes. The gradient in composition results in variations of the absorption coefficient, band gap, intrinsic concentration, and other material parameters, and therefore the complex diffusion equations that yield the quantum efficiency can only be solved using numerical methods. Hence, the study of the quantum efficiency in nonhomogeneous photodiodes is performed separately and will be published elsewhere.

Even though it is shown that the TSF configuration is preferable for photodiodes fabricated on homogeneous material, frequently technological considerations rather than fundamental physical principles dictate the use of the OSF configuration. One of the important technological limitations is that caused by the metal layer which can shield a significant fraction of the incoming light. This limitation, which is usually associated with frontside illumination, can place another limit on the quantum efficiency of both OSF and TSF photodiodes. Consequently, both the TSF and OSF structures are fully analyzed in this paper. The maximal quantum efficiencies as well as the optimal thickness of the absorption volumes, in terms of diffusion lengths, surface recombination velocities, and absorption coefficients, are presented.

II. QUANTUM EFFICIENCY AS A FUNCTION OF ABSORPTION DEPTH

In this section the probability of a minority carrier generated at a distance X_0 from the junction to reach the

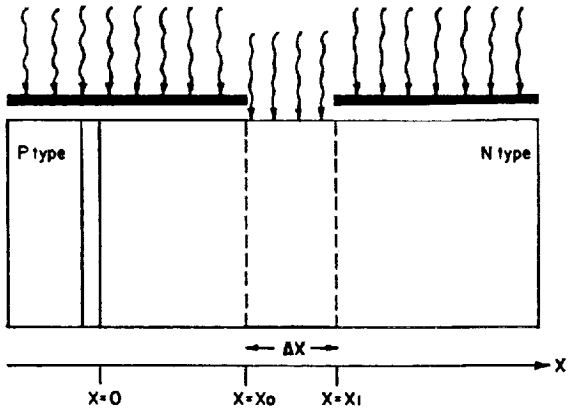

FIG. 2. A photodiode in which the light is uniformly absorbed at a distance of $X_0 < X < X_1$ from the edge of the depletion region.

junction is calculated. This probability is equal to the quantum efficiency associated with photons absorbed at the same distance.

Our assumptions are that both the length and the width of the diode are larger than the diffusion length and therefore the one-dimensional treatment is valid.[5] We also assume low injection conditions, an abrupt junction, a very thin depletion layer, a constant minority-carrier lifetime and a constant dopant concentration along the quasineutral regions.

Let us consider the diode of Fig. 2. Assume that somehow the light is uniformly absorbed only in a narrow n-type volume $A_j\,(X_1-X_0)$ at a distance $X_0<X<X_1$ from the edge of the depletion region. In order to calculate the resulting photocurrent, the steady state of the minority-carrier distribution close to the junction must be found, and therefore the continuity equations for the three regions must be solved,

$$D_p\frac{d^2\hat{p}_1}{dx^2}-\frac{\hat{p}_1}{\tau_p}=0, \qquad 0<x<x_0, \tag{2a}$$

$$D_p\frac{d^2\hat{p}_2}{dx^2}-\frac{\hat{p}_2}{\tau_p}+G_L=0, \qquad x_0<x<x_1, \tag{2b}$$

$$D_p\frac{d^2\hat{p}_3}{dx^2}-\frac{\hat{p}_3}{\tau_p}=0, \qquad x_1<x<d_n, \tag{2c}$$

where p_1, p_2, and p_3 are the minority-carrier concentrations. d_n, D_p, and τ_p represent the width of the neutral region and the minority-carrier diffusion coefficient and lifetime, respectively. The uniform optical generation rate is given by $G_L=N_0/(X_1-X_0)$, where N_0 is the induced photon flux.

The boundary conditions for the problem are

$$\hat{p}_1(0)=\frac{n_i^2}{N_D}\,(e^{qV/kT}-1), \quad \left.\frac{d\hat{p}_3}{dx}\right|_{x=d_n}=\frac{-S_n}{D_p}\hat{p}_3(d_n), \tag{3a}$$

$$\hat{p}_1(x_0)=\hat{p}_2(x_0), \quad \hat{p}_2(x_1)=\hat{p}_3(x_1), \tag{3b}$$

$$\left.\frac{d\hat{p}_1}{dx}\right|_{x=x_0}=\left.\frac{d\hat{p}_2}{dx}\right|_{x=x_0}, \quad \left.\frac{d\hat{p}_2}{dx}\right|_{x=x_1}=\left.\frac{d\hat{p}_3}{dx}\right|_{x=x_1}, \tag{3c}$$

where S_n is the surface recombination velocity. Solving the problem for the short-circuit condition, one obtains for the first zone

$$\hat{p}_1(x)=2A\cosh(x/L_p), \tag{4}$$

$$A=-\frac{N_0L_p^2}{D_p(1+K)}\left(\frac{e^{X_0/L_p}-Ke^{-X_0/L_p}-e^{X_1/L_p}+Ke^{-X_1/L_p}}{(X_1-X_0)}\right),$$

$$K=e^{2(d_n/L_p)}\left(\frac{1+\beta}{1-\beta}\right), \quad \beta=S_nL_p/D_p,$$

where L_p is the diffusion length of the minority carriers, given by $L_p=(D_p\tau_p)^{1/2}$. Knowing $p_1(x)$ the diffusion photocurrent can be obtained by

$$I_\lambda=-qA_jD_p\left.\frac{d\hat{p}_1}{dx}\right|_{x=0}$$

$$=qA_jN_0\left(\frac{e^{X_0/L_p}-Ke^{-X_0/L_p}-e^{X_1/L_p}+Ke^{-X_1/L_p}}{(1+k)(X_1-X_0)/L_p}\right). \tag{5}$$

The term in the large parentheses represents the fraction of holes that is collected by the junction, and forms the photocurrent. This fraction can be treated as the quantum efficiency of the diode, while illuminated in the way shown in Fig. 2. Rewriting the quantum efficiency as

$$\left(\frac{e^{X_0/L_p}-Ke^{-X_0/L_p}-e^{X_1/L_p}+Ke^{-X_1/L_p}}{(1+k)(X_1-X_0)/L_p}\right)$$

$$=\frac{1}{(1+K)}\left(\frac{e^{X_0/L_p}(1-e^{\Delta X/L_p})}{\Delta X/L_p}\right.$$

$$\left.+K\frac{e^{-X_0/L_p}(1-e^{-\Delta X/L_p})}{-\Delta X/L_p}\right), \tag{6}$$

where $\Delta x=X_1-X_0$, and using

$$\lim_{y\to 0}[(1-e^y)/y]=1, \tag{7}$$

we finally obtain

$$\eta'(X_0)=\frac{1}{(1+K)}\,(e^{X_0/L_p}+Ke^{-X_0/L_p}), \tag{8}$$

where η' represents the density of the quantum efficiency of holes generated at a distance X_0 from the edge of the depletion region. It should be emphasized that this quantum efficiency depends on three parameters only: the carrier's initial distance from the depletion region X_0, the parameter β, and the width of the neutral region d_n. It does not depend on the way in which the light is introduced, or on optical parameters such as the absorption coefficient and the photon's energy.

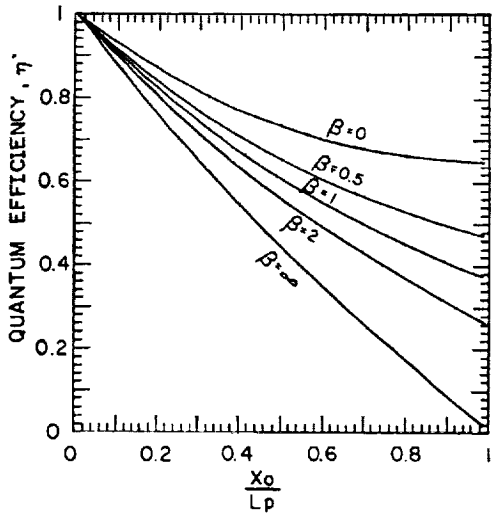

FIG. 3. The quantum efficiency η' given by Eq. (8) as a function of the carrier's initial distance from the junction, with the surface quality as a parameter.

Figure 3 presents the quantum efficiency η' given by Eq. (8) as a function of the distance from the depletion region, with the surface quality as a parameter. It is clearly seen that for all surface conditions, the quantum efficiency dramatically decreases as X_0 increases. Since the distribution of the absorbed photons (and therefore the generated carriers) strongly depends on the way in which the light is introduced, we expect the overall quantum efficiency to be completely different in each configuration. Hence, the preferred side for illumination is the side which is associated with a higher number of photons absorbed close to the junction.

III. THE OVERALL QUANTUM EFFICIENCIES FOR TSF AND OSF CONFIGURATIONS

Let us assume that the photodiodes of Fig. 1 are illuminated with monochromatic photon flux either from their transparent side (a) or from their opaque side (b). Let us further assume that the reflected photon flux in both geometries is negligible. The generation function due to monochromatic photon flux N_0, with wavelength λ, is given in the TSF case by

$$G_L(X,\lambda)=\alpha(\lambda)N_0\,e^{-\alpha(\lambda)X}, \tag{9}$$

where $\alpha(\lambda)$ is the absorption coefficient. Similarly, in the OSF configuration the generation function G_L is given by

$$G_L(X,\lambda)=\alpha(\lambda)N_0\,e^{\alpha(\lambda)(X-d_n)}, \tag{10}$$

where d_n is the width of the quasineutral region.

Since the continuity equation is a linear one, Eqs. (9) and (10) can be used to calculate the quantum efficiencies associated with monochromatic photon flux. For the TSF photodiode the quantum efficiency η_{TSF} is given by

$$\eta_{TSF}(\lambda)=\int_0^{d_n}\alpha(\lambda)e^{-\alpha(\lambda)X}\frac{1}{(1+K)}\left(e^{X/L_p}+Ke^{-X/L_p}\right)dx$$

$$=\frac{\alpha L_p}{1-\alpha^2L_p^2}\left(\frac{-(\beta-\alpha L_p)e^{-\alpha d_n}+\beta\cosh(d_n/L_p)+\sinh(d_n/L_p)}{\cosh(d_n/L_p)+\beta\sinh(d_n/L_p)}-\alpha L_p\right) \tag{11}$$

while for the OSF photodiode the quantum efficiency η_{OSF} is given by

$$\eta_{OSF}(\lambda)=\int_0^{d_n}\alpha(\lambda)e^{\alpha(\lambda)(X-d_n)}\frac{1}{(1+K)}\left(e^{X/L_p}+Ke^{-X/L_p}\right)dx$$

$$=\frac{\alpha L_p}{1-\alpha^2L_p^2}\left(\frac{-(\beta+\alpha L_p)+[\beta\cosh(d_n/L_p)+\sinh(d_n/L_p)]e^{-\alpha d_n}}{\cosh(d_n/L_p)+\beta\sinh(d_n/L_p)}-\alpha L_p\,e^{-\alpha d_n}\right). \tag{12}$$

Equations (11) and (12), which present the quantum efficiency in terms of surface conditions, dimensions, and absorption coefficients, are widely known and used in the literature;[1,7,8] however, they give the quantum efficiency associated with the uncommon case of monochromatic photon flux. HgCdTe photodiodes packaged in infrared imaging systems are usually exposed to radiation emitted from bodies with temperatures of about 300 K. Hence, the flux is usually composed of photons of different wavelengths as described by Plank's radiation law. Therefore, the relevant quantum efficiency for both the OSF and the TSF cases should be obtained by integrating the relative contributions of all photons. While doing so, the dependence of the absorption coefficient on the photons' wavelength should be taken into account (see the Appendix). Hence,

$$\eta_T=\frac{\int_{\lambda_{on}}^{\lambda_{off}}\eta_{TSF}(\alpha,\lambda)n(\lambda,T)d\lambda}{\int_{\lambda_{on}}^{\lambda_{off}}n(\lambda,T)d\lambda}, \tag{13}$$

$$\eta_O=\frac{\int_{\lambda_{on}}^{\lambda_{off}}\eta_{OSF}(\alpha,\lambda)n(\lambda,T)d\lambda}{\int_{\lambda_{on}}^{\lambda_{off}}n(\lambda,T)d\lambda}, \tag{14}$$

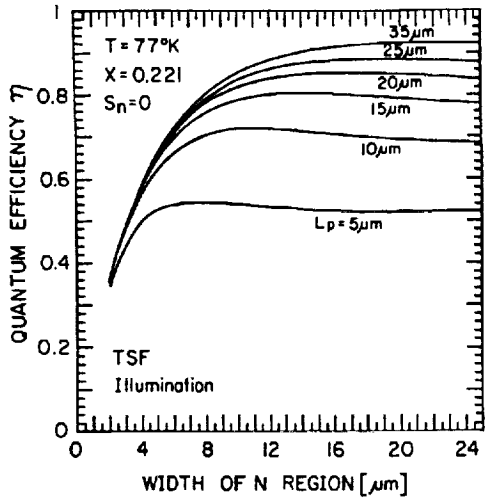

FIG. 4. The quantum efficiency of TSF illuminated $Hg_{1-x}Cd_xTe$ photodiode vs the thickness of the n-type layer with the diffusion length of the holes as a parameter. The bulk composition is $x=0.221$, the hole mobility coefficient is $\mu_p=1000\ cm^2/V\ S$ (Ref. 16) and the surface recombination velocity is $S_n=0$.

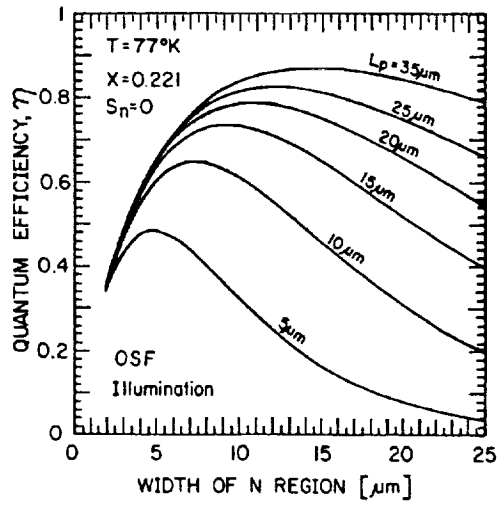

FIG. 5. The same as Fig. 4 for the OSF configuration.

where η_{TSF} and η_{OSF} are given by Eqs. (11) and (12), λ_{on} and λ_{off} are the system's cut-on and cut-off wavelengths, $n(\lambda,T)$ (photons/cm^2 s μm) is the spectral radiant photon emittance of the target as given by Planck's radiation law,[9] and T is the temperature of the target.

IV. RESULTS

Technological considerations rather than fundamental physical principles usually dictate the fabrication of photodiodes based on p-type material, although the longer lifetime of the minority carriers in the n-type material makes it preferable for infrared sensing. However, since our objective is to emphasize the physical and geometrical principles, here we disregard the technological obstacles by assuming that the substrate is a high-quality n-type material. This high-quality material is characterized by high values of both mobility and lifetime of the minority carriers. In addition, we assume in our two example photodiodes excellent surface recombination velocities in both diodes, which yield electrical reflecting conditions for the holes. Hence, the two above-mentioned photodiodes differ only in the direction of illumination.

Figures 4 and 5 show the quantum efficiencies obtained in the two configurations as calculated from Eqs. (13) and (14). Both figures show the quantum efficiency versus the width of the absorption volume with the diffusion length of the minority carriers as a parameter. The hole mobility coefficient was assumed to be $\mu_p=1000\ cm^2/V\ S$ (Ref. 10) and the surface recombination velocity was assumed to be very low ($S_n=0$). The hole lifetime varies from 38 nS up to 2 μS which yields minority diffusion lengths from 5 up to 35 μm. We chose $Hg_{1-x}Cd_xTe$ with $x=0.221$ which yields a reasonable value for the cut-off wavelength (11 μm) for a hole lifetime of 100 nS, at 77 K.[11] Consequently, λ_{on} and λ_{off} were taken to be 8 and 11 μm, respectively.

The superiority of the TSF photodiode in the case of reflecting surface conditions is clearly seen. To begin with, the quantum efficiency obtained for the TSF photodiode is always larger than that obtained for the OSF photodiode. In the case of the material with a minority-carrier diffusion length of 35 μm, the maximal quantum efficiencies obtained are 92% and 87%, for the TSF and OSF configuration, respectively. For materials with shorter diffusion lengths the relative difference between the two configurations is even more significant. For example, in the case where $L_p=5$ μm, the maximal values of the quantum efficiencies were 54% and 48%, for the TSF and OSF configurations, respectively.

In addition to the differences in the values of the quantum efficiency, the difference in the sensitivity of the two photodiodes to the width of the n-type layer is obviously noticed. It is clearly seen that in the case of the OSF configuration there is an "optimal" thickness of the n-type layer for each value of the diffusion length. It is also clearly seen that the quantum efficiency is rapidly degrading as the n-type layer thickness deviates from its optimal value; however, in the case of the TSF configuration the quantum efficiency reaches a saturation value which is very close to the maximal value. Therefore, the term "optimal thickness" of the n-type layer, used in the OSF illuminated diode, is not valid, and the term "minimal thickness" should be applied.

The strong dependence of the quantum efficiency on the width of the absorption region, as it exists in OSF illuminated photodiodes, is a serious limitation, since the width of the n-type region can vary along an array of photodiodes. This results in a severe nonhomogeneity in the quantum efficiencies and in the performance of the photodiodes. This yields a significant degradation in the system's figures of merit, such as NET.[12,13]

Excellent surface conditions in HgCdTe are not easily

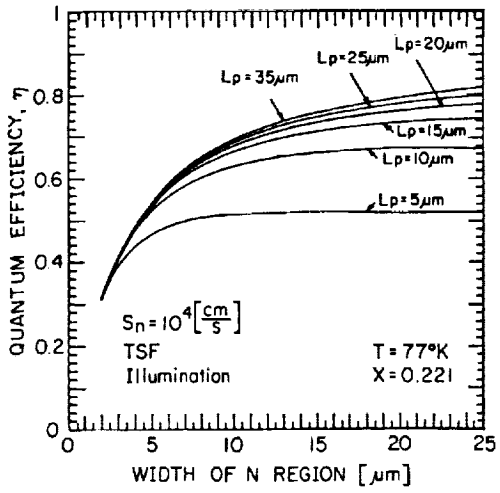

FIG. 6. The same as Fig. 4 but $S_n = 10^4$ cm/s.

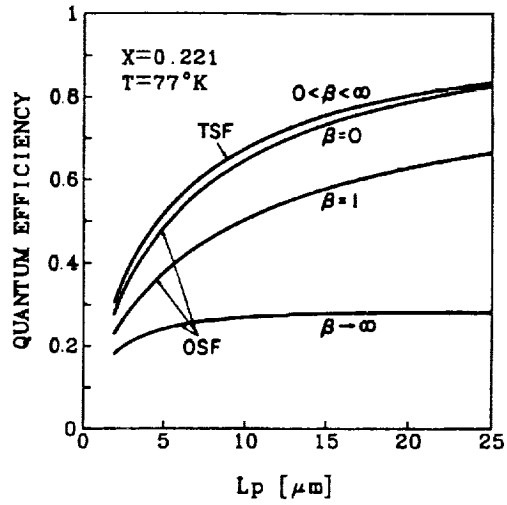

FIG. 8. The maximal quantum efficiency obtained for the OSF case with β as a parameter, and the saturation value of the quantum efficiency obtained for the TSF case.

achieved.[14] Most of the published data concerning the surface recombination velocity in n-type material is related to photoconductors. Since the photoconductors require accumulation conditions, the reported data is of no value to $Hg_{1-x}Cd_xTe$ photodiodes with $x \cong 0.2$, which require a weak depletion condition.[15] Hence, we chose the surface recombination velocity in our example diodes to be 10^4 cm/S, which is a practical value for p-type material.[16]

Figures 6 and 7 show the quantum efficiencies obtained for $S_n = 10^4$ cm/s in the two configurations. Once again, the superiority of the TSF configuration (in terms of high quantum efficiency and homogeneity) is seen very clearly. In addition to the two above-mentioned advantages of the TSF configuration, Figs. 4–7 demonstrate a third one: The TSF illuminated diodes reach a saturation value, and

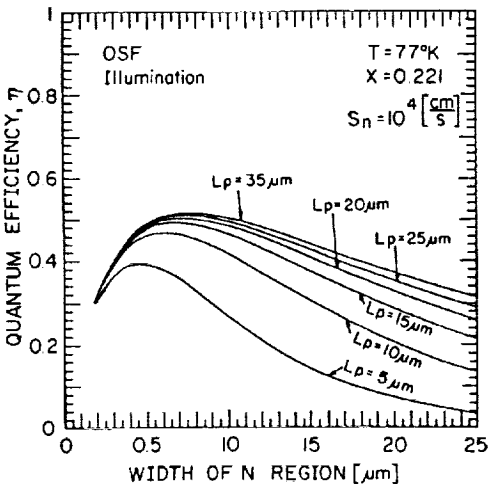

FIG. 7. The same as Fig. 6 for the OSF configuration.

therefore are less sensitive to the surface recombination velocity in the edge of the n-type layer.

Figure 8 shows the maximal quantum efficiency obtained for the OSF configuration with β as a parameter, as well as the saturation value of the quantum efficiency obtained for the TSF case (which is close to the maximal value). It should be noted, however, that the surface recombination velocity S_n is not constant along the horizontal axis since the diffusion length is changing, and $S_n = (\beta D_p / L_p)$, as indicated by Eq. (4). Figure 8 demonstrates clearly the two advantages of the TSF illumination case: For the same quality of the material (i.e., the same diffusion length) the quantum efficiency associated with the TSF case is always higher than that associated with the OSF case, and does not depend upon the surface condition.

Figure 9 shows the optimal thickness of the n-type layer versus the hole diffusion length with $\beta = 0$, for both TSF and OSF cases. It should be mentioned that in the OSF case, the width drawn in Fig. 9 is the optimal width, and the quantum efficiency rapidly degrades when a different width is applied. In the TSF case, however, the plotted width is the minimal width, and the associated quantum efficiency remains constant for values higher than the minimum.

Figure 9 indicates an additional advantage of the TSF case. For the same diffusion length the thickness of the optimal absorption region associated with the TSF configuration is smaller than that associated with the OSF configuration; hence, there is less diffusion leakage current in the TSF diode.

V. SUMMARY

We have presented a theoretical study of the quantum efficiency of HgCdTe photodiodes fabricated on thin films, with the objective to emphasize the geometrical depen-

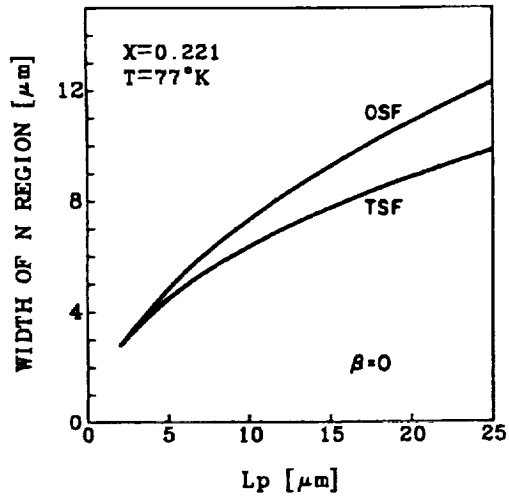

FIG. 9. The thickness of the n-type layer (for which the maximal quantum efficiencies are obtained), vs the diffusion lengths of the holes. This thickness is the minimal thickness in the TSF case, and the optimal thickness in the OSF case.

dence of the quantum efficiency and to determine whether the OSF or TSF configuration is preferable. In particular, we calculated the probability of a carrier to be collected at the junction as a function of its initial distance from the edge of the depletion region. Using the above probability function, we pointed out the importance of inducing absorption close to the junction and suggested that the light should be absorbed after it passes through the transparent region (TSF). Following that, we have calculated the quantum efficiencies for both TSF and OSF illuminated diodes, and showed that the quantum efficiencies associated with the TSF configuration are always higher than those associated with the OSF configuration. In addition, we pointed out the difference in the sensitivity to the thickness of the absorption region. Our calculations show that the quantum efficiency in the OSF instance is dramatically degraded when the absorption thickness differs from the optimal one. We have also shown that, in the TSF case, the quantum efficiency reaches a saturation value, and therefore does not depend on the thickness of the absorption region. Our final conclusion is that the TSF illuminated diodes are much superior sensors for IR thermal imaging.

ACKNOWLEDGMENTS

The authors wish to thank Y. Betser for his help with the numerical calculations, S. Schacham for his helpful remarks, and P. Eliyau for her technical assistance. The editorial assistance of I. Rosenfeld is also acknowledged with thanks.

APPENDIX

The absorption coefficient in semiconductor materials such as HgCdTe is given for energies higher than the band gap by

$$\alpha(x,T,E)=\gamma(E-E_g)^{1/2}, \tag{A1}$$

where E is the energy of the photon, E_g is the band gap, and γ is a coefficient that depends on the material and temperature only. Radiation is absorbed also at energies lower than the band gap, a process known as the Urbach tail.[17] The absorption coefficient associated with the Urbach tail in HgCdTe is given by[18]

$$\alpha(x,T,E)=\alpha_0 e^{[\sigma(E-E_0)/W]}, \tag{A2}$$

where x is the composition, T is the temperature, E is the energy of the photon, and α_0, σ, W, and E_0 are fitting parameters. Finkman and Schacham[19] measured the absorption coefficient over the temperature range 80 K $< T <$ 300 K and obtained

$$E=hc/\lambda \ \text{(eV)},$$

$$\alpha_0=\exp(53.61x-18.88) \ (\text{cm}^{-1}),$$

$$\sigma=3.267\times10^4(1+x) \ \text{(K/eV)},$$

$$W=81.9+T \ \text{(K)},$$

$$E_0=1.838x-0.3424+0.148x^4 \ \text{(eV)}.$$

In a previous work[20] an expression for γ was derived, based on the assumption that the absorption coefficient and its derivative are continuous. Hence,

$$\gamma=(2\sigma e/W)^{1/2}\alpha_0 e^{[\sigma(E_g-E_0)/W]}, \tag{A3}$$

where e is the base of the natural logarithm.

[1] F. van der Wiele, in *Solid State Imaging*, edited by P. G. Jespers, F. van der Wiele, and M. H. White (Leydon, Noordhoff, 1976), p. 47.
[2] A. Rogalsky and J. Rutkowski, Infrared Phys. 22, 199 (1982).
[3] J. Shappir and A. Kolodny, IEEE Trans. Electron Devices ED-24, 1093 (1977).
[4] D. Levy, S. E. Schacham, and I. Kidron, IEDM Tech. Dig. 18, 373 (1986).
[5] D. Levy, S. E. Schacham, and I. Kidron, IEEE Trans. Electron Devices ED-34, 2059 (1987).
[6] R. J. Briggs, IEDM Tech. Dig., p. 165 (1981).
[7] M. B. Reine, A. K. Sood, and T. J. Tredwell, in *Semiconductors and Semimetals*, edited by R. K. Willarson and A. C. Beer (Academic, New York, 1981), Vol. 18, Chap. 6.
[8] E. Zand and Y. Nemirovsky, Infrared Phys. 25, 591 (1985).
[9] J. M. Lloyd, *Thermal Imaging Systems* (Plenum, New York, 1975).
[10] Y. Shacham-Diamond and I Kidron, J. Appl. Phys. 56, 1104 (1984).
[11] Y. Nemirovsky and D. Rosenfeld, J. Appl. Phys. 63, 2435 (1988).
[12] F. D. Shepherd, Proc. SPIE 930, 2 (1988).
[13] N. Bluzer, Proc. SPIE 930, 64 (1988).
[14] Y. Nemirovsky and G. Bahir, J. Vac. Sci. Technol. A 7, 450 (1989).
[15] G. Bahir and D. Rosenfeld (unpublished).
[16] E. Finkman and S. E. Schacham, J. Vac. Sci. Technol. A 7, 464 (1989).
[17] F. Urbach, Phys. Rev. 92, 1324 (1953).
[18] E. Finkman and Y. Nemirovsky, J. Appl. Phys. 50, 4356 (1979).
[19] E. Finkman and S. E. Schacham, J. Appl. Phys. 56, 2896 (1984).
[20] D. Rosenfeld, D.Sc. thesis, Technion—I.I.T, Haifa, Israel, 1989.

SECTION THREE

HIGH TEMPERATURE SUPERCONDUCTIVITY